Journal of Enzyme Inhibition and Medicinal Chemistry

www.tandfonline.com/ienz
ISSN: 1475-6366 (print), 1475-6374 (electronic)

J Enzyme Inhib Med Chem, 2016; 31(S2): 51–62
 DOI: 10.1080/14756366.2016.1187143

Taylor & Francis
Taylor & Francis Group

RESEARCH ARTICLE

A substituted sulfonamide and its Co (II), Cu (II), and Zn (II) complexes as potential antifungal agents

Jorge R. A. Diaz[1], Martín Fernández Baldo[2], Gustavo Echeverría[3], Héctor Baldoni[4], Daniela Vullo[5], Delia B. Soria[6], Claudiu T. Supuran[5], and Gerardo E. Camí[1]

[1]INTEQUI (CONICET, CCT-San Luis), Área de Química General e Inorgánica, Facultad de Química, Bioquímica y Farmacia, Universidad Nacional de San Luis, San Luis, Argentina, [2]INQUISAL (CONICET, CCT-San Luis), Departamento de Química, Facultad de Química, Bioquímica y Farmacia, Universidad Nacional de San Luis, San Luis, Argentina, [3]LANADI – IFLP (CONICET, CCT-La Plata), Departamento de Física, Facultad de Ciencias Exactas, Universidad Nacional de La Plata, La Plata, Argentina, [4]Instituto de Matemática Aplicada San Luis (IMASL-CONICET), Universidad Nacional de San Luis, San Luis, Argentina, [5]Neurofarba Department, University of Florence, Sesto Fiorentino (Firenze), Italy, and [6]CEQUINOR (CONICET, CCT-La Plata), Departamento de Química, Facultad de Ciencias Exactas, Universidad Nacional de la Plata, La Plata, Argentina

Abstract

A sulfonamide 1-tosyl-1-*H*-benzo(*d*)imidazol-2-amine (TBZA) and three new complexes of Co(II), Cu(II), and Zn(II) have been synthesized. The compounds have been characterized by elemental analyses, FTIR, ^{1}H, and ^{13}C-NMR spectroscopy. The structure of the TBZA, and its Co(II) and Cu(II) complexes, was determined by X-ray diffraction methods. TBZA and its Co(II) complex crystallize in the triclinic *P*-1 space group, while the Cu(II) complex crystallizes in the monoclinic $P2_1/c$ space group. Antifungal activity was screened against eight pathogenic yeasts: *Candida albicans* (DMic 972576), *Candida krusei* (DMic 951705), *Candida glabrata* (DMic 982882), *Candida tropicalis* (DMic 982884), *Candida dubliniensis* (DMic 93695), *Candida guilliermondii* (DMic 021150), *Cryptococcus neoformans* (ATCC 24067), and *Cryptococcus gattii* (ATCC MYA-4561). Results on the inhibition of various human (h) CAs, hCA I, II, IV, VII, IX, and XII, and pathogenic beta and gamma CAs are also reported.

Keywords

Antifungal, carbonic anhydrase, metal complex, sulfonamide, thermal stability

History

Received 19 April 2016
Revised 3 May 2016
Accepted 4 May 2016
Published online 24 May 2016

Introduction

Sulfonamide inhibitors of the metalloenzyme carbonic anhydrase (CA, EC 4.2.1.1) such as acetazolamide (AZA) have been used clinically as diuretics, antiglaucoma, or anticonvulsant agents for long periods[1–9], whereas more recent drug design studies have evidenced other CA inhibitors (CAIs) belonging to the sulfonamide/sulfamate/sulfoamide classes as molecules of interest for developing novel therapies for obesity[10,11] and cancer[12–15]. They are based on the selective inhibition of CA isozymes involved in those pathologies. To date, 15 such isoforms have been described in humans[1,16].

Invasive fungal infections constitute an ever-increasing cause of morbidity and mortality among immunocompromised individuals, those who have undergone intra-abdominal surgery, neonates, and the elderly[17]. While fluconazole remains an important agent for the treatment of *Candida* and other yeasts infections, the introduction of other triazoles active against yeasts and molds, such as posaconazole, and voriconazole, or drugs belonging to other classes, such as echinocandin, anidulafungin, caspofungin, and micafungin, has increased the options for prophylaxis, and therapy of many fungal infections[18,19].

Address for correspondence: Gerardo E. Camí. E-mail: gecami@unsl.edu.ar

Another important pathogen in oral health is *Porphyromonas gingivalis*, coccobacillus gram-negative, immobile, strictly anaerobic, responsible for diseases such as chronic periodontitis. It has also been identified as a risk factor for lung infections, in immunocompromised patients, preterm births, and other diseases[20]. A CA enzyme called PgiCA present in *P. gingivalis*, belonging to the gamma CA class, has been investigated for its inhibition profile with sulfonamides and other compounds[21]. Thus, the mechanism of sulfonamides action for inhibiting the growth and development of strains of this microorganism has been proposed as a new antiinfective strategy.

In this work, the synthesis of TBZA, a new sulfonamide and its three metal complexes with Co(II), Cu(II) and Zn(II) is presented. Furthermore, the crystal structures of TBZA, Co(II), and Cu(II) complexes are reported, as well as a complete characterization of the four solid phases. Based on the biological tests, the possible effectiveness of these new compounds as antifungal agents is discussed, evaluating whether the mechanism of action of carbonic anhydrase enzyme is involved. The antifungal activity of these new compounds was also assessed *ex vivo*.

Experimental

Materials

All reagents were supported by Sigma-Aldrich and Merck.

Synthesis

The sulfonamide synthesis was performed in one stage[22] by the dissolution of 0.5 g (2.624 mmol) of *p*-toluenesulfonyl chloride, 100 mg (0.82 mmol) of 4-dimethylaminopyridine (4-DMAP) and 0.3 mL (3.57 mmol) of Et_3N as catalysts, in 30 mL of dry CH_2Cl_2 at room temperature and under Ar environment (Figure 1). Once dissolved, 0.4 g (3 mmol) of 2-aminobenzimidazole was added to the reaction mixture. The reaction was controlled using TLC, and when it was complete, the solvent was removed under vacuum, and then, 1-M HCl was added to remove catalyst and excess reagents. The white solid obtained was recrystallized from absolute ethanol, very slowly evaporating the solvent at 15 °C and protecting compound from direct light. A week later, yellowish transparent needle-like TBZA crystals appeared, and some of them were selected for structural determination by single crystal XRD. The yield of the reaction was 85%. The elemental analysis resulted as follows: C 61.2% (*c*a. 58.54%), H 5.1% (*ca*. 4.53%), N 12.8% (*ca*. 14.63%), S 9.7% (*ca*. 11.15%), and O 11.2% (*ca*. 11.15%). Sulfanilamide was used as reference.

The Cu(II) complex was obtained by dissolving 17.0 mg (0.1 mmol) of $CuCl_2.2H_2O$ in 20 mL of absolute ethanol, and subsequently, 57.4 mg (0.2 mmol) of sulfonamide was added. The appearance of a dark green color in the final solution was observed. The Co(II) complex was obtained by dissolving 23.8 mg (0.1 mmol) of $CoCl_2.6H_2O$ in 20 mL of absolute ethanol, subsequently adding 57.4 mg (0.2 mmol) sulfonamide. A dark blue color in the final solution was observed. The Zn(II) complex was obtained by dissolving 15.4 mg (0.1 mmol) of $ZnCl_2.H_2O$ in 20 mL of absolute ethanol, and then adding 57.4 mg (0.2 mmol) of sulfonamide. This resulted in a full dissolution, leaving a clear colorless solution. Mother-waters were filtered to let them crystallize two weeks, obtaining dark green crystals (in the case of the Cu(II) complex), prismatic crystals of intense blue color (in the case of the Co(II) complex), and a white crystalline precipitate in the case of the Zn(II) complex. Some single crystals of Co(II) and Cu(II) complexes were selected for single crystal XRD structural determination. The average yield in the obtaining of the complexes was 65%. The result of elemental analysis was: C 49.8% (*ca.* 47.74%), H 4.7% (*ca.* 3.69%), N 10.2% (*ca.* 11.93%), S 7.5% (*ca.* 9.09%), and O 10.1% (*ca.* 9.09%) in Co(II) complex; C 50.5% (*ca.* 47.43%), H 5.1% (*ca.* 3.67%), N 11.2% (*ca.* 11.86%), S 7.8% (*ca.* 9.03%), and O 10.7% (*ca.* 9.03%) in Cu(II) complex; C 48.8% (*ca.* 47.30%), H 4.6% (*ca.* 3.66%), N 10.7% (*ca.* 11.82%), S 8.1% (*ca.* 9.01%), and O 10.0% (*ca.* 9.01%) in Zn(II) complex. Sulfanilamide was used as reference. The difference found in the corresponding measures for the Cu(II) complex is due to the incorporation of butane in the crystal structure, located randomly at holes. Butane was included in the used solvent for their synthesis (ethanol). The approximate ratio of butane is 2.9% of the total mass of C, H, and O (Table 1).

Methods

The measurements were performed on an Oxford Xcalibur, Eos, Gemini CCD diffractometer with graphite-monochromated CuKα ($\lambda = 1.54184$ Å) radiation for TBZA and the Cu(II) complex, and MoKα ($\lambda = 0.71073$ Å) radiation for the Co(II) complex. The X-ray diffraction intensities were collected (ω scans with θ and κ-offsets), integrated and scaled with CrysAlisPro[23] suite of programs. The unit cell parameters were obtained by least-squares refinement (based on the angular settings for all collected reflections with intensities larger than seven times the standard deviation of measurement errors) using CrysAlisPro. Data were corrected empirically for absorption, employing the multi-scan method implemented in CrysAlisPro. The structure was solved by direct methods with SHELXS-97, and the molecular model was refined by full-matrix least-squares procedure on F^2 with SHELXL-97 of the SHELX package[24] within the WinGX program[25].

Except for amide hydrogen atoms, which were positioned from the Fourier difference map, all H-atoms were positioned on stereo-chemical basis, and refined with the riding model. The methyl H-atoms were refined as rigid groups allowed to rotate around their corresponding C – C bond such as to maximize the sum of the observed residual electron density at their calculated positions. The structural analysis was performed using the SHELX package[24], PLATON[26], and Mercury[27], available within the WinGX program.

The experimental XRPD patterns were obtained on a diffractometer Rigaku D-MAX-IIIC with Cu Kα ($\lambda = 1.5418$ Å) radiation. The data were collected over a range of 10–40° (2θ) with a step of 2°; the effective counting time was 5 s per step.

The elemental analyses (C, H, N, S) were carried out with a Carlo Erba EA 1108 microanalyser belonging to the Instituto de

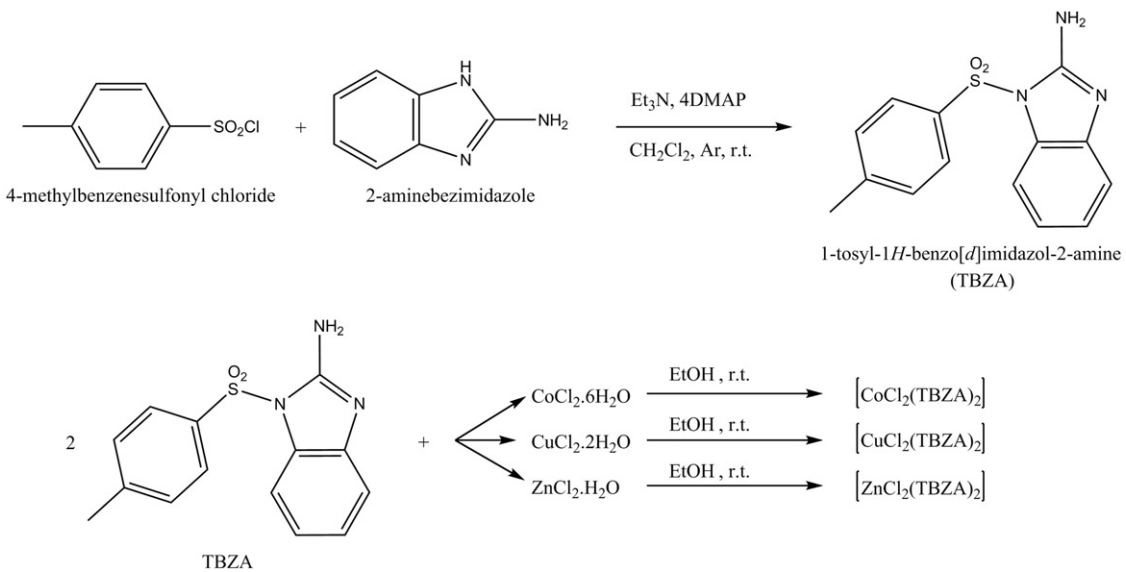

Figure 1. Synthesis of TBZA and its Co(II), Cu(II), and Zn(II) complexes.

Table 1. Crystal data and structure refinement for TBZA (**1**) and its Cu(II) (**2**) and Co(II) (**3**) complexes.

Complex	**1**	**2**	**3**
Empirical formula	$C_{28}H_{26}N_6O_4S_2$	$C_{30}H_{31}Cl_2CuN_6O_4S_2$	$C_{28}H_{26}Cl_2CoN_6O_4S_2$
Formula weight	574.67	738.17	704.50
T (K)	297(2)	297(2)	297(2)
Wavelength (Å)	1.54184	1.54184	0.71073
Crystal system	Triclinic	Triclinic	Monoclinic
Space group	*P*-1	*P*-1	$P2_1/c$
Unit cell (Å, °)			
a	9.7806(6)	11.3456(6)	9.9125(4)
b	10.3229(6)	12.5730(6)	15.9355(7)
c	14.8434(7)	12.6348(6)	19.4059(7)
α	80.942(4)	68.044(5)	90.0
β	71.444(5)	85.608(4)	92.188(4)
γ	86.248(4)	71.760(4)	90.0
V (Å^3)	1402.8(1)	1585.94(15)	3063.1(2)
Z	2	2	4
ρ_{calc} (g·cm^{-3})	1.360	1.546	1.528
μ (mm^{-1})	2.1	4.1	0.916
F(000)	600	760	1444
Crystal size (mm)	$0.478 \times 0.207 \times 0.158$	$0.077 \times 0.169 \times 0.290$	$0.274 \times 0.183 \times 0.143$
θ-range	3.174 to 74.027	3.984 to 73.438	2.995 to 29.378
Index ranges			
	$-10 \le h \le 11$	$-14 \le h \le 13$	$-12 \le h \le 13$
	$-12 \le k \le 12$	$-15 \le k \le 14$	$-21 \le k \le 11$
	$-18 \le l \le 17$	$-15 \le l \le 15$	$-26 \le l \le 25$
Collected	9366	11 933	15 170
Unique	5556 ($R_{int} = 0.0231$)	6261 ($R_{int} = 0.0255$)	6981 ($R_{int} = 0.0345$)
Completeness	99.9% ($\theta = 67.684°$)	100.0% ($\theta = 67.684$)	99.8%(θ =25.242)
Observed [I > 2σ(I)]	4709	5178	4811
Absorption correction		Semi-empirical from equivalents	
T_{max}/T_{min}	1.00000/0.83686	1.00000/0.77619	1.00000/0.96054
Data/restraints/parameters	5556/0/364	6261/1/409	6981/5/406
Goodness-of-fit on F^2	1.077	1.091	1.049
R_1/wR_2 [I > 2σ(I)]	0.0408/0.1200	0.0424/0.1163	0.0480/0.0962
R_1/wR_2 (all data)	0.0486/0.1273	0.0521/0.1259	0.0838/0.1122
Extinction coefficient	0.0116(6)	–	–
$\Delta\rho_{max}/\Delta\rho_{min}$ (e.Å^{-3})	0.243/−0.299	0.382/−0.427	0.357/−0.390

Química Física de Materiales, Medio Ambiente y Energía (INQUIMAE), Universidad de Buenos Aires, Argentina. Sulfanilamide was used as standard.

Fourier-transformed infrared (FT-IR) spectra were recorded on a Nicolet Protégé 460 spectrometer provided with a CsI beamsplitter in the 4000–250 cm^{-1} range with 32 scans and spectral resolution of 4 cm^{-1}, using KBr pellet technique.

Thermogravimetric (TGA) and differential thermal analysis (DTA) curves were obtained with a Shimadzu TGA-51 Thermal Analyzer and DTA-50 Thermal Analyzer, using platinum pans, flowing air at 50 mL min^{-1} and a heating rate of 10 °C min^{-1} from room temperature to 1000 °C. The Differential Scan Calorimeter analyses (DSC) were performed with a Shimadzu DSC-60, using aluminum pans, flowing air at 50 mL min^{-1}, and a heating rate of 10 °C min^{-1} from room temperature to 600 °C.

To confirm melt or crystalline phase changes, a Leitz Westlar heating microscope stage was used.

The ^{1}H and ^{13}C-NMR were obtained by a NMR Bruker Avance 200 MHz spectrometer with a BBI 200 MHz S1 5-mm probe with gradient in z axis.

Computation

The experimental geometries (i.e. XRD and XRPD) obtained for the TBZA complexes (TBZA-M(II)) were characterized at the DFT level of theory by using the B3LYP exchange-correlation functional. B3LYP is a popular density functional of broad application with a good performance for weak interaction calculation[28–30]. The Stuttgart/Dresden electron core potential method SDD (ECP) basis set was selected for Co(II), Cu(II), and Zn(II) atoms, while the 6–311G + (2d,p) basis set was used for all other atoms.

The geometries of the complexes were fully optimized with no symmetry constraint and tight convergence criteria, followed by normal vibrational frequency calculations using the same method and basis set in order to characterize the stationary points as minima (no imaginary frequencies), and to obtain their zero-point vibrational energies. All calculations were carried out with the Gaussian 09 package[31].

In order to characterize the nature and strength of the TBZA-M(II) formation, QTAIM[32,33] analyses was done with the wave function obtained by single-point calculations using a larger 6–311G + (2d,p):Def2-QZVP basis sets.

By the QTAIM analysis, the nature and strength of atomic interactions were studied and classified[34]. This was carried out by analyzing the topological properties of the *ab initio* wave function according to the Bader's theory[32,33]. In brief by the QTAIM theory, the molecular wave function can be partitioned into atomic basins. Therefore, the strength of the interactions between atoms trough the analysis of local properties at the bonding critical points (BCPs) can be identified and characterized. The QTAIM analysis was carried out with the AIMPAC suite of programs[35–37].

Microorganisms

For the antifungal activity study, the following yeasts of clinical relevance were assayed; *Candida albicans* (DMic 972576), *Candida krusei* (DMic 951705), *Candida glabrata* (DMic 982882), *Candida tropicalis* (DMic 982884), *Candida dubliniensis*

(DMic 93695), *Candida guilliermondii* (DMic 021150), *Cryptococcus neoformans* (ATCC 24067), and *Cryptococcus gattii* (ATCC MYA-4561). These yeasts were grown on potato dextrose agar (PDA) at 37 °C for 48–72 h. The isolates were maintained on PDA at 4 °C for further studies. The yeast strains were provided by the Department of Mycology of the National Institute of Infectious Diseases by Dr. Carlos G. Malbrán, Argentina.

Assessment of the antifungal activity

For the assessment of the antifungal activity, 200 µL of yeast (2.0×10^6 yeast mL^{-1}) of each studied strain was aseptically inoculated into PDA plates. Cavities of 3 mm were made and were filled with 50 µL of TBZA and its complexes. The plates were incubated at 37 °C for 48 h. After incubation, the zones of inhibition were measured. In addition, voriconazole and fluconazole were used as positive controls. The assays were performed in triplicate, and the values were expressed in millimeters.

CA inhibition

An Applied Photophysics stopped-flow instrument was used for assaying the CA-catalyzed CO_2 hydration activity[38]. Phenol red (at 0.2 mM) was used as indicator, working at the absorbance maximum of 557 nm with 10-mM Hepes (pH 7.4) or TRIS (pH 8.3) as buffers and 0.1-M $NaClO_4$ (for maintaining constant ionic strength) at 20 °C, following the CA-catalyzed CO_2 hydration reaction for a period of 10–100 s (the uncatalyzed reaction needed around 60–100 s in the assay conditions, whereas the catalyzed ones were of around 6 – 10 s), as described earlier[39–46]. The CO_2 concentrations ranged from 1.7 to 17 mM for the determination of the kinetic parameters. The uncatalyzed rates were similarly determined and subtracted from the total observed rates. Enzyme concentrations in the assay system range of 10–25 nM for all the enzymes considered in the present study, which have been obtained as recombinant proteins, in-house, as reported earlier[46–51].

Results and discussion

Sulfonamide characterization

An ORTEP[52] plot of the TBZA molecule is shown in Figure 2, and in Table 1, some significant structural parameters are listed. Bond intramolecular phenyl ring distances, similar to those found in Cu(II) and Co(II) complexes, were in the range of 1.364(3) to 1.415(3) Å, as expected for the resonant bond structure of these cyclic groups. TBZA crystallized with two independent molecules in the asymmetry unit, differing from one another in the tosyl and 2-aminobenzimidazole group arrangement (Table 2). In addition, they are nearly perpendicular; the intramolecular angles between aromatic rings were 88.86(6)° and 86.72(8)°.

A network of intermolecular H-bonds further stabilized the structure (Table 3). Two benzimidazole groups related by an inversion center, which laid over the same plane, are connected by a double H-bond involving one of the amine hydrogen and the imidazole nitrogen atoms. Beside, the other amine hydrogen atom establishes a bifurcated H-bond interaction with sulfonyl oxygen atoms belonging to the same molecule, and to a symmetry-related molecule[53].

Figure 3 shows the FTIR spectra of the sulfonamide and their complexes with divalent ions; and Table 4 presents the assignment of most important vibrational modes[54]. The 2-amino group (benzimidazole ring) presents an asymmetric stretching at 3467–3453 cm^{-1} and a symmetrical one at 3317 cm^{-1}. Low-intensity

Table 2. Selected bond lengths (Å), angles and torsional angles (°) for TBZA (**1**) and its Cu(II) (**2**) and Co(II) (**3**) complexes.

	1	2	3
*Bonds**			
N11–M		1.983(2)	2.015(2)
N21–M		1.990(2)	2.023(2)
Cl1–M		2.2154(9)	2.3488(1)
Cl2–M		2.2471(8)	2.2327(10)
*Bond angles**			
N21–M–N11		98.13(9)	110.19(10)
Cl1–M–N11		101.10(6)	105.55(7)
Cl2–M–N11		129.52(7)	107.43(7)
Cl1–M–N21		132.69(7)	108.88(7)
Cl2–M–N21		98.67(7)	110.00(7)
Cl1–M–Cl2		101.43(4)	114.66(4)
Torsional angles			
C14–N13–S111–C114	79.0(2)	61.9(2)	60.4(2)
C24–N23–S211–C214	70.8(2)	91.4(2)	80.5(3)

*M = Cu1 or Co1.

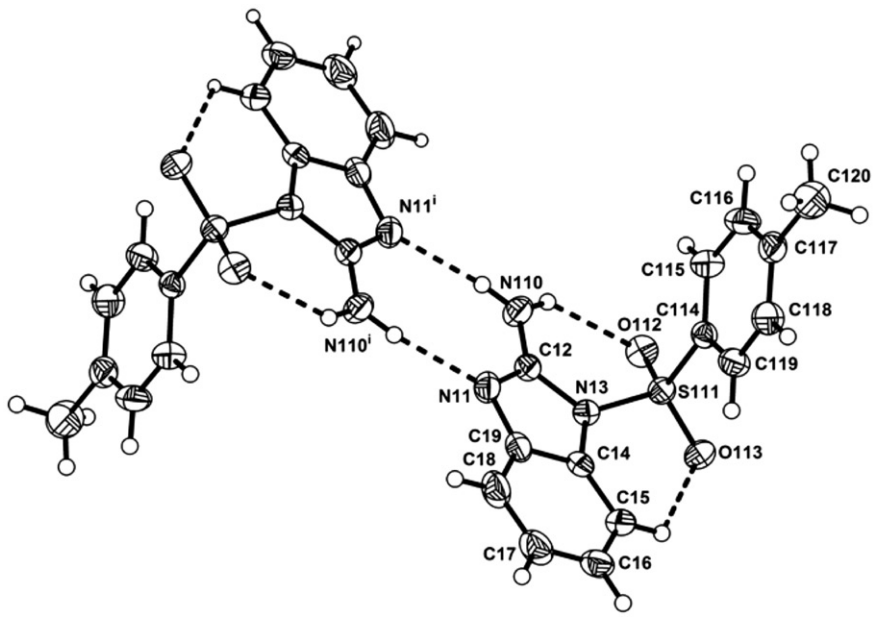

Figure 2. View of the two TBZA showing one of the independent molecules together with its symmetry-related by an inversion center. Displacement ellipsoids are drawn at the 30% probability level, and the intra and intermolecular H-bonds are shown in dashed line. Symmetry operations are listed in Table 3.

Table 3. Selected intra and intermolecular hydrogen bonds for TBZA (**1**) and its Cu(II) (**2**) and Co(II) (**3**) complexes (Å and °).

D–H···A	Compound	D–H	H···A	D···A	D–H···A
Intramolecular H–bonds					
N110–H1AA···Cl1	**2**	0.76	2.48	3.165(2)	148.9
	3	0.85(1)	2.37(2)	3.170(3)	157(3)
N210–H2AA···Cl2	**2**	0.83	2.46	3.169(3)	143.3
	3	0.85(1)	2.39(1)	3.201(3)	161(3)
	1	0.86	2.14	2.802(2)	133.5
N110–H1AB···O112	**2**	0.80	2.11	2.768(3)	138.5
	3	0.85(3)	2.09(2)	2.724(4)	130(3)
	1	0.93	2.49	3.043(3)	118.2
C25–H25···O213	**2**	0.88	2.47	2.978(4)	117.4
	3	0.93	2.45	3.014(5)	118.7
	1	0.86	2.13	2.788(3)	133.2
N210–H2AB···O212	**2**	0.67	2.34	2.829(4)	131.7
	3	0.85(1)	2.11(3)	2.764(4)	133(3)
	1	0.93	2.42	2.977(3)	118.5
C15–H15···O113	**2**	0.91	2.56	3.112(4)	119.2
	1	0.93	2.49	3.043(3)	118.2
C25–H25···O213	**2**	0.88	2.47	2.978(4)	117.4
	3	0.93	2.45	3.014(5)	118.7
Intermolecular H–bonds					
N110–H1AB···N11^{i}	**1**	0.86	2.09	2.941(3)	171.2
N210–H2AA···N21^{ii}	**1**	0.86	2.17	3.024(3)	170.9
N210–H2AB···O112^{iii}	**1**	0.86	2.38	2.940(2)	123.2
C115–H115···O212^{iv}	**2**	0.93	2.52	3.398(4)	157.1
C15–H15···Cl1^{v}	**3**	0.93	2.94	3.595(3)	128.9
C219–H219···O113^{vi}	**3**	0.93	2.65	3.384(4)	135.9
C32–H32C···Cl2^{vii}	**2**	0.96	2.34	3.069(6)	132.3

Symmetry transformations used to generate equivalent atoms: (i) $-x+2, -y+1, -z$; (ii) $-x, -y+2, -z+1$; (iii) $x-1, y+1, z$; (iv) $x+1, y, z$; (v) $x-1, y, z$; (vi) $-x, y-1/2, -z+1/2$; (vii) $-x+1, -y+2, -z+1$.

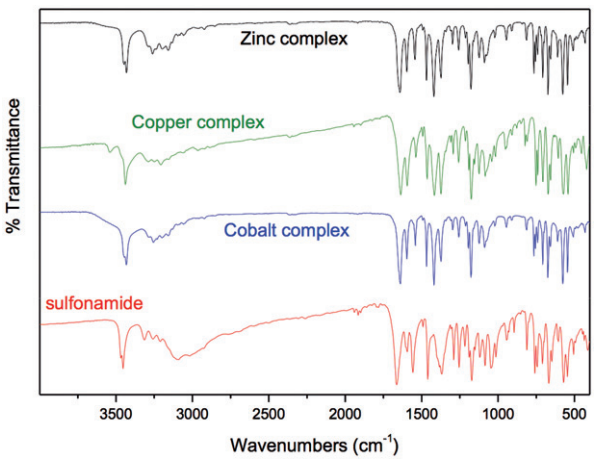

Figure 3. FTIR spectra of TBZA, Co(II) complex, Cu(II) complex, and Zn(II) complex.

wide bands, appearing at 3261 and 3211 cm^{-1}, were attributed to of H-bonds, according to what is observed in the crystal structure. They involve the azole nitrogen of the benzimidazole ring and the 2-amino group. The angular deformation of 2-amino group was observed at 1595 cm^{-1}. The observed bands at 1664, 1558, 1491, and 1461 cm^{-1} correspond to different C-N stretching, associated with angular deformation of the methyl group. Bands appearing at 1372 and 1174 cm^{-1} correspond to the asymmetric and symmetric stretching of the sulfonamide sulfonyl group. The band appearing at 945 cm^{-1} corresponds to the S-N stretching of the sulfonamide. The assignment of the rest of the bands is presented in Table 3.

The ^{1}H-NMR spectrum shows two protons of the 2-amino group (benzimidazole ring) as a singlet which integrates two protons, with a chemical shift of 6.9 ppm. The ^{13}C-NMR spectrum shows the quaternary carbon bound to 2-amino group presenting a chemical shift of 152.1 ppm. The two quaternary carbons linking six-and five-membered rings of the benzimidazole ring have a chemical shift of 142.0 ppm and 130.5 ppm. The other carbons of the benzimidazole ring are seen as doublets at 116.6 ppm, 121.5 ppm, 124.8 ppm, and 112.5 ppm; corresponding protons (located in the same order) are observed at 7.29 ppm (*d*, 7.7 Hz), 7.21 ppm (*td*, 7.7 Hz, 1.4 Hz), 7.10 ppm (*td*, 7.7 Hz, 1.4 Hz), and 7.73 ppm (*d*, 7.7 Hz). The quaternary carbons of tosyl group are seen at 134.5 and 146.1 ppm. The carbon of methyl group is observed as a quadruplet at 21.6 ppm, and its protons as a singlet at 2.37 ppm. The two carbons which are attached to the quaternary carbon sulfonyl group are observed as a doublet at 127 ppm and protons at 7.86 ppm (*d*, 8.3 Hz). The two carbons below the quaternary carbon, which is bonded to methyl, are observed as a doublet at 130.2 ppm and protons at 7.26 ppm (*d*, 8.3 Hz). To achieve this assignment, the ^{1}H, HSQC, and HMBC calculations were performed (see figures in Supplementary Material).

Figure 4(a) shows the sulfonamide thermal diagrams (DTA – TGA). The compound is stable up to 190 °C. There is, then, a first endothermic process without loss of mass (on set 196.69 °C), which is assigned to the fusion of the sulfonamide. This fact was confirmed using a microscope with heating plate, noting the merger between 198 and 200 °C. Then, there is an exothermic peak (on set 237.04 °C) with a loss of mass of 6.64% (*ca.* 5.23%) corresponding to the loss of the terminal methyl of the tosyl group. This is followed by an endothermic process (on set 349.06 °C) with a loss of mass of 46.52% (*ca.* 45.99%), due to the decomposition of the 2-aminobenzimidazole ring. Finally an exothermic process happens (on set 566.74 °C) with a loss of mass of 46.84% (*ca.* 48.78%); no waste from calcination is observed (see Figure 5).

Complex characterization

Figures 6 and 7 display ORTEP diagrams for the coordination of the TBZA ligand around Cu(II) and Co(II) metals.

Table 4. Proposed FTIR assignment of TBZA and its metal complexes.

Mode	TBZA (cm^{-1})	Co(II) complex (cm^{-1})	Cu(II) complex (cm^{-1})	Zn(II) complex (cm^{-1})
νO–H	–	–	3539 (w)	–
νNH_2	3467–3453 (s)	3444–3430 (s)	3439 (s)	3444–3430 (s)
νNH	3317–3261–3211 (m)	3288–3256–3234–3200 (m)	3291–3250–3208 (m)	3288–3256–3234–3200 (m)
νCH_{ar}	3159 (sh)–3097–3091 (m)–3021 (w)	3159 (m)–3097 (w)–3081–3057 (w)–3033 (sh)	3158–3110–3063–3032 (w)	3159 (m)–3097 (w)–3081–3057 (w)–3033 (sh)
νCH_{al}	2977–2940 (w)–2876–2807 (w)	2979–2961 (w)–2923–2853 (w)	2982–2965–2921 (w)–2887–2862 (vw)	2979–2961 (w)–2923–2853 (w)
δNH_2	1664 (s)	1640 (s)	1639 (s)	1640 (s)
νCN	1597 (m)–1558 (s)–1461 (s)	1597 (s)–1540 (m)–1468 (s)	1595 (s)–1539 (m)–1464 (s)	1597 (s)–1540 (m)–1468 (s)
δCH	1491 (vw)–1397–1386 (m)–1308 (vw)	1491 (vw)–1420 (s)–1344–1310 (vw)–1299 (w)	1494 (vw)–1419 (s)–1344–1308 (vw)–1294 (m)	1491 (vw)–1420 (s)–1344–1310 (vw)–1299 (w)
$\nu_{as}SO_2$	1372 (s)	1374 (s)	1374 (s)	1374 (s)
νCC	1288 (m)–1255 (s)–1218 (m)–1191–1152–1121 (m)	1256 (m)–1213 (w)–1194 (m)–1159 (sh)–1124 (m)	1257 (m)–1213 (m)–1191–1154–1124 (m)	1256 (m)–1213 (w)–1194 (m)–1159 (sh)–1124 (m)
$\nu_s SO_2$	1174 (s)	1175 (s)	1177 (s)	1174 (s)
δCH + νCC	1087–1046–1040–1015 (m)	1089 (m)–1076 (sh)–1052 (sh)–1022 (w)	1085–1043–1018 (m)	1089 (m)–1076 (sh)–1052 (sh)–1022 (w)
νSN	945 (m)	945 (w)	951 (m)	945 (w)
δCH	931–895–853–812 (w)–745–711 (m)–697 (sh)	912 (w)–765–740–708 (m)	909–878 (w)–851–809 (m)–739–708 (s)	912 (w)–765–740–708 (m)
δNH	812 (m)–759 (s)	813 (m)–754 (m)	823 (m)–752 (s)	813 (m)–754 (m)
$\delta \Sigma O_2$	670 (s)	673 (s)	672 (s)	673 (s)
νCS	608 (m)	609 (m)	607 (m)	609 (m)
Red modes	650 (m)–572 to 302 (w)	657 (m)–577 to 304 (w)	657 (m)–633 (vw)–574 to 300 (w)	657 (m)–577 to 304 (w)

ν: stretching, δ: bending, ar: aromatic, al: aliphatic, as: asymmetric, s: symmetric; (s): strong, (m): medium, (w): weak, (vw): very weak, (sh): shoulder.

Bond distances, bond angles, and some relevant intermolecular distances are listed in Table 2. In both complexes, metal centers are tetrahedrally coordinated by two chloride atoms and two azole nitrogen atoms from the benzimidazole ring. Even though the Cl1-Co1-Cl2 angle, 114.66(4)°, is larger than the corresponding one in Cu(II) complex, 101.43(4)°, presumably due to a larger electronic chloride cloud repulsion, the coordination sphere of the Cu(II) complex has the largest distortion from the regular tetrahedron.

Similar to the TBZA in solid state, benzimidazole and tosyl ring groups are located approximately perpendicular to each other, with angles of 81.50(7)° and 86.0(1)° in the Cu(II) complex, and of 83.20(8)° and 86.0(1)° in the Co(II) complex. These results could be rationalized taking into account that beside the intramolecular H-bond established by the 2-amino group of the benzimidazole ring with the oxygen atoms of the sulfonyl group (observed also in TBZA), the 2-amino group is involved in an intramolecular H-bond with chloride ion, while in TBZA (as discussed above) it is connected to an imidazole nitrogen atom of a neighbor molecule (Table 3). The crystal structures of both complexes are stabilized by a network of nonconventional H-bonds which involve tosyl or benzimidazole carbon atoms as proton donors with sulfonyl or chloride atoms as proton acceptors (Table 3). Moreover, molecules in the Cu(II) complex pack, forming a channel parallel to the crystallographic *a* axis, where butane molecules are linked by H-bonds with chloride ions bonded to the metal centers.

The FTIR spectra show a characteristic spectroscopic pattern for each complex. However, a qualitative similarity can be seen in the spectra of the Co(II) and Zn(II) complexes (Figure 3). The great similarity of the infrared spectra, even at low frequencies, leads us to infer that the Co(II) and Zn(II) complexes are isostructural. The three complexes show that the group amino is not involved in the coordination of the central ion, since νNH modes do no shift significantly with respect to the free sulfonamide. However, a decrease of approximately 25 cm^{-1} with respect to the free sulfonamide νNH evidences a slight weakening of the bond NH by interaction with chloride ions (Table 4). The bands observed at 1640, 1540, and 1420 cm^{-1} show complexation through azolic nitrogen, because they are assigned to the νC-N stretching modes, and are weakened in the three complexes with respect to the values observed in the free sulfonamide.

The thermal behavior of the complexes shows similar patterns of decomposition. Figure 4(b–d) presents the thermal diagrams of Co(II), Cu(II), and Zn(II) complexes, respectively.

Unlike the free sulfonamide that melts and then decomposes, the complexes melt and decompose immediately. The three complexes underwent a first endothermic process followed by an exothermic one with loss of mass, which in the case of the complex of Co(II) was 3.24%, (c.a. 4.25%, on set 148.42 °C), for Cu(II) complex was 4.94% (c.a. 4.14%, on set 259.82 °C), and for Zn(II) complex was 5.45% (c.a. 4.22%, on set 263.42 °C). This mass loss is assigned to the loss of the methyl of the tosyl group, as it is the case with the sulfonamide. Then, a series of exothermic and endothermic processes followed, in which the loss was between 20 and 30% of the mass. It can be estimated that two chlorides and sulfonyl groups were lost, representing, in the case of the Co(II) complex, a loss of mass of 28.08% (*ca.* 29%, on set 250.18 °C), in the case of the Cu(II) complex, 29.78% (*ca.* 29%, on set 285.06 °C), and in the case of the Zn(II) complex, 29.17% (*ca.* 29%, on set 334.12 °C). Two exothermic processes followed from 480 °C approximately, where the 58.28% (on set 480.16 °C) of the mass for the Co(II) complex, the 55.43% (on set 478.00 °C) of mass for the Cu(II) complex, and the 56.48% (on set 475.94 °C) of the mass for the Zn(II) complex were lost. This similarity in the

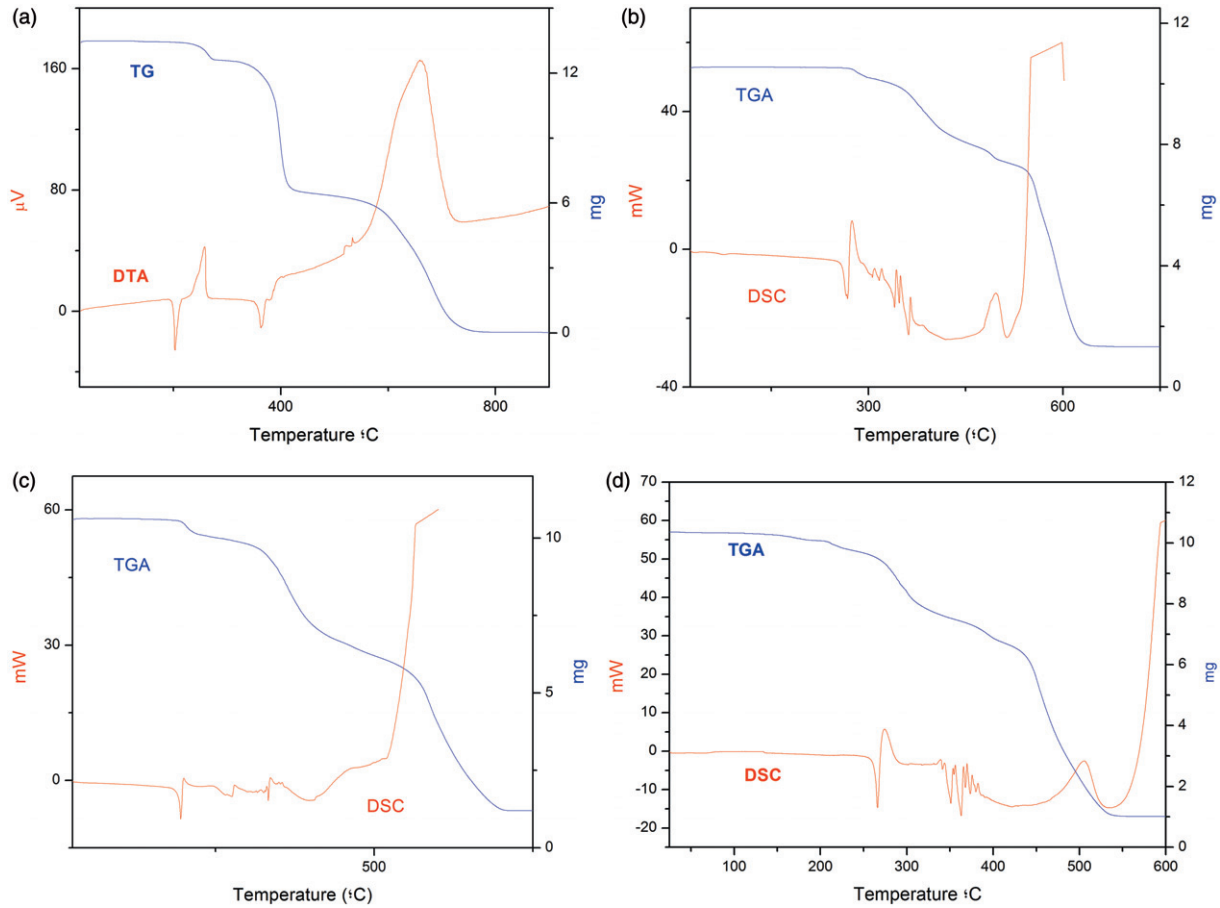

Figure 4. (a) DTA–TGA graphics of TBZA; (b) DSC–TGA graphics of Co(II) complex; (c) DSC–TGA graphics of Cu(II) complex; (d) DSC–TGA graphics of Zn(II) complex.

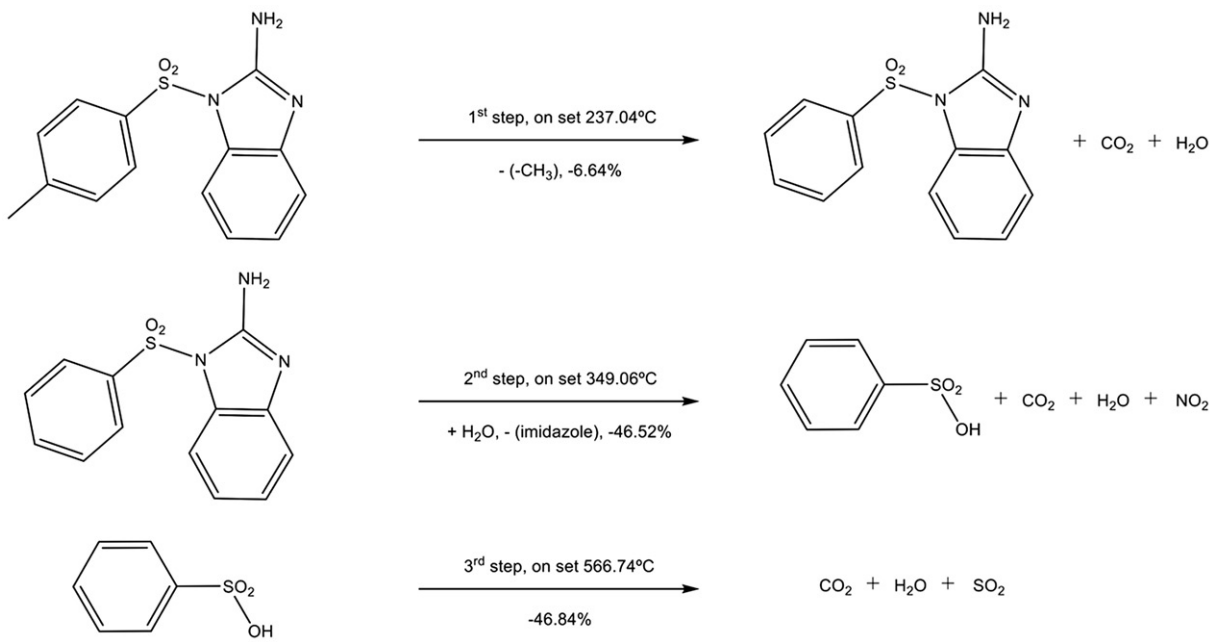

Figure 5. Proposed decomposition of TBZA..

thermal behaviors indicates that the structure of the complexes is similar, according to their crystal structures. This agreement leads us to further infer that the Zn(II) complex can be isostructural to Co (II) complex.

The residues remaining after calcination were measured using XRD powder. The diffractograms obtained are in agreement with the corresponding Co(II) (PDF# 00–009-0402), Cu(II) (PDF# 00–005-0661), and Zn(II) (PDF# 00–005-0664) oxides.

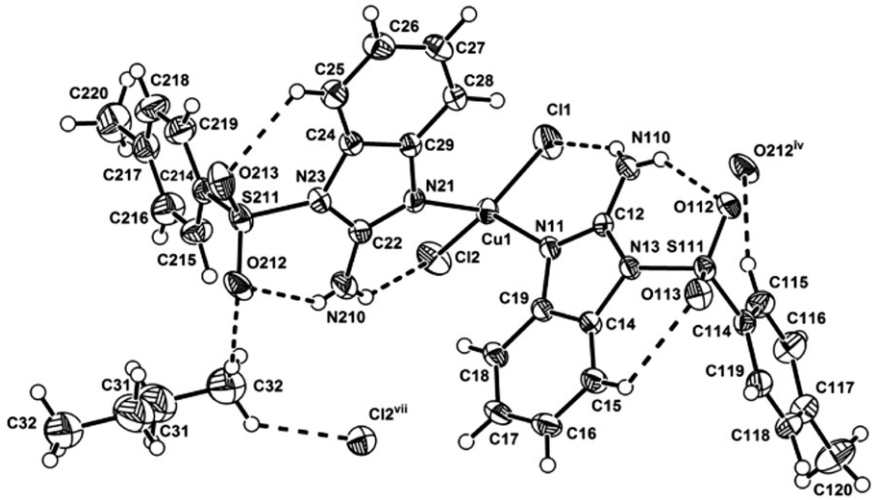

Figure 6. Coordination of the TBZA ligand around the Cu(II) metal center, showing the displacement ellipsoids at the 30% probability level. The intra and intermolecular H-bonds are shown in dashed line. Symmetry operations are listed in Table 3.

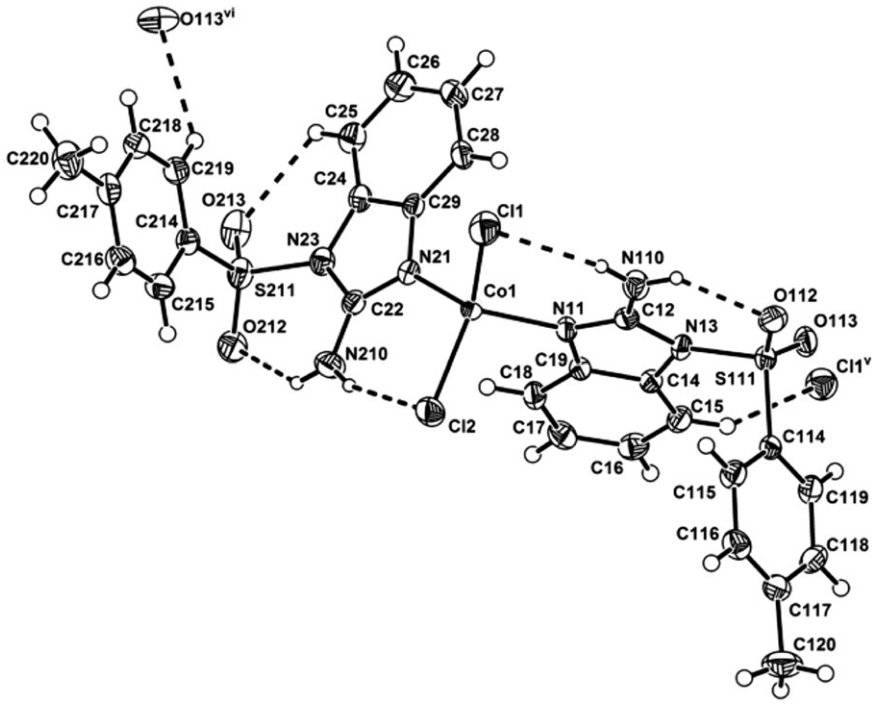

Figure 7. Coordination of the TBZA ligand around the Co(II) metal center, showing the displacement ellipsoids at the 30% probability level. The intra and intermolecular H-bonds are shown in dashed line. Symmetry operations are listed in Table 3.

When measuring Zn(II) and Co(II) complexes, the XRD powder showed that the crystalline phases were equivalents (but not coincident). As there are coincidences in the crystallographic planes, we may say that both phases are isostructural (Figure 8). This fact confirms what has been inferred in the analysis of FTIR spectra, elemental analysis, and thermal diagrams.

DFT calculations

Geometry

Full geometry optimizations of the single crystal XRD coordinates (complexes TBZA-Cu(II) and TBZA-Co(II)) and the proposed coordinates for the TBZA-Zn(II) complex assumed from it XRPD spectra were carried out. The B3LYP functional with the 6–311G + (2d,p) and SDD(ECP) basis sets was selected for the TBZA and M(II) moieties, respectively. Geometry optimizations were carried out by global energy minimization without any structural constraint followed by frequencies analysis

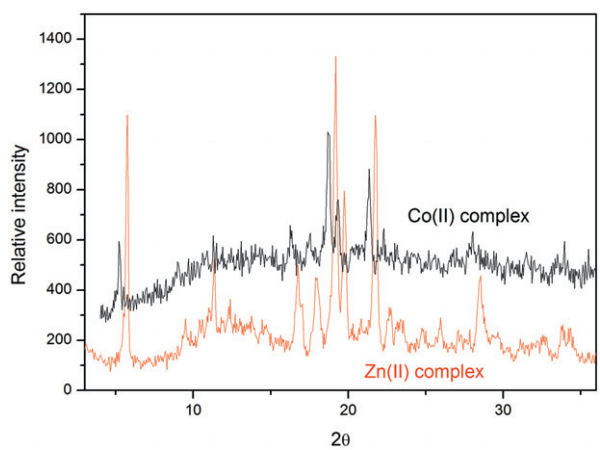

Figure 8. Powder XRD of Co(II) complex and Zn(II) complex.

to characterize the final structures as global minimum. No negative frequencies were found.

In order to obtain a feeling for the overall discrepancies between the experimental and the optimized coordinates, and to assess the influence of the selected DFT functional and basis set, we have measured the overall RMSD between the energy minimized structures with respect to the corresponding experiment coordinates. The minimized structures showed RMSD of 0.605, 0.935, and 0.673 angstroms for the TBZA-Zn(II), TBZA-Cu(II), and TBZA-Co(II) complexes, respectively. Thus, the final DFT geometries correspond closely with the experimental data. We assumed that no significant structural drift from its starting crystallographic coordinates occurred. According to these results, the conformations obtained by DFT geometry optimization were taken to perform the subsequent QTAIM analysis.

QTAIM analysis

The nature and strength of the metal–ligand bond for the TBZA-M(II) were investigated in the light of the QTAIM theory[32,33], using the B3LYP/6–311 + G(2d,p):Def2-QZVP wave function. Selected topological parameters are listed in Table 5. The number of critical points (CP) found for all of the analyzed systems are in agreement with the Poincare–Hopf rule[32], indicating not only that the complexes are well stabilized in terms of electron density distribution but also pointing out that the free TBZA can be stabilized by M(II) complexation, at least for Co(II), Cu(II), and Zn(II) ions.

N–M(II) (N11–M(II), N21–M(II)) interaction

From Table 5, it can be seen that the values of ρ are in a range from 0.0783 to 0.0849 au, and the values of $\nabla^2\rho$ are positive, whereas the number of electron pairs shared between the two atomic basins are $\delta(A,B) < 1$. These results indicate a close-shell interaction at the BCP[55]. Concordantly, the amount of kinetic energy per electron is large, $G/\rho > 1$. In fact, the N–M(II) interaction might be classified as dative bonding ($V < 0$, and $H < 0$) although some amount of covalence might be present, playing, sometimes, a fundamental role.

Cl–M(II) (Cl1–M(II), Cl2–M(II)) interaction

The values of ρ are in a range from 0.0642 to 0.0657 au, with positive values of $\nabla^2\rho$. The number of electron pairs shared by two atomic basins is $\delta(A,B) > 1$, with an amount of kinetic energy per electron (G/ρ) lower than the unity (Table 5). These results indicate a shared-shell interaction at the Cl–M(II) BCP, and might be classified as covalent bonding ($V < 0$, and $H < 0$)[55].

The topological results reinforce the fact that the TBZA complexes are better stabilized at the N–M(II) BCP by close-shell dative bonding with a slightly covalent character.

Biological assays

Antifungal activity

The antifungal activity of TBZA and its complexes was evaluated against different strains of yeasts of clinical relevance, such as *C. albicans* (DMic 972576), *C. krusei* (DMic 951705), *C. glabrata* (DMic 982882), *C. tropicalis* (DMic 982884), *C. dubliniensis* (DMic 93695), *C. guilliermondii* (DMic 021150), *C. neoformans* (ATCC 24067), and *C. gattii* (ATCC MYA-4561). The results obtained with the studied compounds are presented in Table 6.

Regarding the antifungal activity, these compounds demonstrated to be effective against the assayed yeasts. The maximum zones of inhibition for TBZA, its Co(II), Cu(II), and Zn(II)

Table 5. Topological properties at the BCP for selected binuclear interactions.

BCPa	R_e [b,j]	ρ [c,k]	$\nabla^2\rho$ [d,k]	G [e,k]	G/ρ [f,k]	V [g,k]	H [h,k]	$\delta(A,B)$ [i,k]
N_a···Zn(II)	2.053	0.0783	0.2972	0.0947	1.2094	–0.1152	–0.0204	0.8574
N_b···Zn(II)	2.053	0.0784	0.2975	0.0949	1.2104	–0.1154	–0.0205	0.8589
Cl_a···Zn(II)	2.309	0.0657	0.1726	0.0608	0.9254	–0.0785	–0.0177	1.1112
Cl_b···Zn(II)	2.308	0.0656	0.1725	0.0608	0.9268	–0.0784	–0.0176	1.1110
N_a···Cu(II)	2.017	0.0848	0.3282	0.1075	1.2676	–0.1329	–0.0254	0.9694
N_b···Cu(II)	2.017	0.0849	0.3282	0.1075	1.2661	–0.1329	–0.0254	0.9689
Cl_a···Cu(II)	2.316	0.0650	0.1627	0.0587	0.9030	–0.0768	–0.0180	1.2344
Cl_b···Cu(II)	2.316	0.0650	0.1627	0.0587	0.9030	–0.0768	–0.0180	1.2345
N_a···Co(II)	2.038	0.0812	0.3576	0.1107	1.3633	–0.1320	–0.0213	0.9312
N_b···Co(II)	2.038	0.0812	0.3574	0.1107	1.3633	–0.1320	–0.0213	0.9311
Cl_a···Co(II)	2.325	0.0642	0.1796	0.0629	0.9797	–0.0809	–0.0180	1.2028
Cl_b···Co(II)	2.325	0.0642	0.1796	0.0629	0.9797	–0.0809	–0.0180	1.2029

[a]BCP involving M(II) ion; [b]distance between nuclei; [c]electron density and [d]its Laplacian ($\nabla^2\rho$); [e]kinetic electron energy; [f]kinetic energy per electron; [g]potential electron energy; [h]total electron energy density (G + V); [i]delocalization index. [j]in Å; [k]in a.u.

Table 6. Antifungal activity of TBZA and its complexes, voriconazole (VNZ), and fluconazole (FNZ).

Tested fungal strains	[a]TBZA (83 μg)	[a]TBZA Co(II) complex (5 μg)	[a]TBZA Cu(II) complex (5 μg)	[a]TBZA Zn(II) complex (5 μg)	[a]VNZ (1 μg)	[a]FNZ (25 μg)
Candida albicans	10 ± 3	12 ± 2	12 ± 2	17 ± 2	25 ± 4	20 ± 5
Candida krusei	10 ± 2	17 ± 2	14 ± 1	15 ± 3	23 ± 3	15 ± 3
Candida glabrata	13 ± 3	15 ± 1	12 ± 2	18 ± 2	24 ± 4	22 ± 3
Candida tropicalis	15 ± 2	12 ± 2	13 ± 2	20 ± 3	23 ± 6	22 ± 4
Candida dubliniensis	10 ± 2	14 ± 1	14 ± 2	14 ± 2	25 ± 5	20 ± 5
Candida guilliermondii	12 ± 1	12 ± 2	12 ± 2	22 ± 3	26 ± 4	22 ± 5
Cryptococcus neoformans	18 ± 3	20 ± 3	15 ± 1	22 ± 3	24 ± 5	20 ± 4
Cryptococcus gattii	13 ± 2	15 ± 1	15 ± 3	15 ± 2	25 ± 5	20 ± 5

All values represented in the table are average of results of three separately conducted experiments.
[a]Zone of inhibition (mm), [a]X ± SD, mean of five measurements ± standard deviation.

complexes were observed against *Cryptococcus neoformans* (18 ± 3, 20 ± 3, 15 ± 1, and 22 ± 3 mm, respectively) compared with the other yeasts investigated in the present study. Moreover, several studies of antifungal activity using $CoCl_2$, $CuCl_2$, and $ZnCl_2$ commercial salts were performed against the same tested yeasts. The results of these studies did not show zones of inhibition (data not shown).

These results strongly suggest that the TBZA and its complexes may possess a significant antifungal activity. However, further studies should be performed to understand the toxicity of the studied compounds before developing these novel substances for clinical applications.

CA inhibition

Inhibition data with TBZA salts against various human (h) CAs, hCA I, II, IV, VII, IX, and XII, and pathogenic beta and gamma CAs, have been obtained. Acetazolamide, a well-known CAI, was used as a standard drug for comparison (Table 7). As in other CAs inhibition assays with sulfonamides and their metal complexes, phenols, and thiophenols, the enzymes were incubated for 10–15 min with test compounds to allowing the formation of the enzyme-inhibitor adduct[44–48,56–60]. Working under similar conditions, TBZA, Co(II), Cu(II), and Zn(II) complexes were found to be poor inhibitors of both hCAs and microorganisms CAs in the micromolar concentration range, although they exhibited a very weak inhibitory power compared to AZA (Table 7). However, an exception occurs with *P. gingivalis* CA γ, where good inhibitory action was observed (Table 8). These results show that the interaction of the sulfonamide with the active site of the enzyme is weaker (than it is for AZA), due to the fact that the TBZA is a substituted sulfonamide and it does not allow the stabilization adduct between the Zn (II) active site of the enzyme and TBZA or its metal complexes. This is consistent with the X-ray crystal structures, in which the deprotonated sulfonamide group appears bound to the Zn(II) ion from the enzyme active site[7,47,48].

In previous studies, it was found that, by inhibiting CAs from bacterial or other pathogens, an inhibition in the growth of the studied microorganisms occurred[41,48,49]. Table 8 shows the values of enzyme inhibition for CAs in *P. gingivalis* (responsible for periodontal pathogenicity) and *Cryptococcus neoformans* (responsible for serious, systemic fungal diseases)[1,7,8]. According to these values, the best results were obtained against PgiCAgamma. Thus, the TBZA may be considered an interesting candidate for possible application in designing antiinfective agent with a novel mechanism of action against *P. gingivalis*.

Table 7. Inhibition data of the studied compounds against various human (h) CAs, hCA I, II, IV, VII, IX, and XII. AZA (Acetazolamide), a well-known CAI, was used as a standard for comparison.

	K_I (nM)					
Compound	hCA I	hCA II	hCA IV	hCA VII	hCA IX	hCA XII
TBZA	>50 000	4700	>50 000	2560	7100	405
Co(II) complex	8700	380	670	870	3200	800
Cu(II) complex	>50 000	>50 000	560	765	930	846
Zn(II) complex	>50 000	>50 000	740	980	4600	930
AZA	250	12	–	–	25	5.70

Table 8. Inhibition of pathogenic beta and gamma CAs.

	K_I (μM)		
Compound	Can2	PgiCAbeta	PgiCAgamma
TBZA	>50	>50	8.30
Co(II) complex	>50	>50	>50
Cu((II) complex	>50	>50	>50
Zn(II) complex	>50	>50	>50

PgiCA is the CA from *Porphyromonas gingivalis*; Can2, the beta CA from *Cryptococcus neoformans*.

Conclusions

This study reports the synthesis and characterization of a new sulfonamide and its Co(II), Cu(II), and Zn(II) complexes. The TBZA and Co(II) and Cu(II) complexes were structurally characterized for the first time via X-ray crystallography. The spectroscopy properties resulted in good agreement with the X-Ray crystallographic results, and in the Zn(II) complex, these studies suggest that it is isostructural with Co(II) complex.

The DFT geometries corresponded closely with the experimental data and no significant structural drift from its crystallographic coordinates occurred. From the QTAM analysis, we can rationalize that the N–M(II) interaction might be classified as dative bonding with some amount of covalence, while the QTAIM analysis of the Cl–M(II) interaction indicates a covalent bonding. In addition, from the ρ and δ(A,B) values, we may assume that the TBZA–M(II) complexes become stabilized following the delocalization index trend, $Cu(II) \approx Co(II) > Zn(II)$.

The TBZA and its complex demonstrated that, *in vitro*, they have a clear antifungal activity against the assayed yeasts. However, TBZA and the Zn(II) complex showed a higher inhibition than the other complexes.

All the compounds showed a lower CA inhibitory property than AZA. However, TBZA presented the highest inhibitory activity against hCA XII. The hCA II results for Cu(II) complex suggest that the inhibitory activity is probably due to the metal ion and not to the TBZA. The results of the enzymatic inhibition in *C. neoformans* and *P. gingivalis* indicate that the CA inhibition is not responsible for the growing yeast inhibition, but TBZA is an effective inhibitor of the gamma CA of the *P. gingivalis*.

Acknowledgements

The authors thank Dr. P. Rossomando (UNSL) for his NMR facilities.

Declaration of interest

The authors report no conflicts of interest. The authors alone are responsible for the content and writing of this article.

This work is supported by the research project PROICO 2–1612, UNSL (director: Dr. G. E. Narda), by the UNLP, by CONICET (PIP 1529), and by ANPCyT (PME06 2804 and PICT06 2315) of Argentina. M.F.B., G.E., H.B., and D.B.S. are members of CONICET.

References

1. Supuran CT. Carbonic anhydrases: novel therapeutic applications for inhibitors and activators. Nat Rev Drug Discov 2008;7:168–81.
2. Neri D, Supuran CT. Interfering with pH regulation in tumours as a therapeutic strategy. Nat Rev Drug Discov 2011;10:767–77.
3. Supuran CT, Scozzafava A, Conway J, editors. Carbonic anhydrase—its Inhibitors and activators. Boca Raton (FL), New York, London: CRC Press; 2004:1–363
4. Temperini C, Cecchi A, Scozzafava A, Supuran CT. Carbonic anhydrase inhibitors. Sulfonamide diuretics revisited-old leads for new applications? Org Biomol Chem 2008;6:2499–506.
5. Pastorekova S, Parkkila S, Pastorek J, Supuran CT. Carbonic anhydrases: current state of the art, therapeutic applications and future prospects. J Enzyme Inhib Med Chem 2004;19:199–229.
6. Supuran C.T., Scozzafava A., Casini A. Development of sulfonamide carbonic anhydrase inhibitors. In: Supuran CT, Scozzafava A,

Conway J, editors. Carbonic anhydrase—its inhibitors and activators. Boca Raton (FL): CRC Press; 2004:67–147
7. Supuran CT. Structure-based drug discovery of carbonic anhydrase inhibitors. J Enzyme Inhib Med Chem 2012;27:759–72.
8. Supuran CT. Carbonic anhydrases: from biomedical applications of the inhibitors and activators to biotechnological use for CO(2) capture. J Enzyme Inhib Med Chem 2013;28:229–30.
9. Nishimori I, Onishi S, Takeuchi H, Supuran CT. The alpha and beta classes carbonic anhydrases from *Helicobacter pylori* as novel drug targets . Curr Pharm Des 2008;14:622–30.
10. Casini A, Antel J, Abbate F, et al. Carbonic anhydrase inhibitors: SAR and X-ray crystallographic study for the interaction of sugar sulfamates/sulfamides with isozymes I, II and IV. Bioorg Med Chem Lett 2003;13:841–5.
11. De Simone G, Di Fiore A, Menchise V, et al. Carbonic anhydrase inhibitors. Zonisamide is an effective inhibitor of the cytosolic isozyme II and mitochondrial isozyme V: solution and X-ray crystallographic studies. Bioorg Med Chem Lett 2005;15: 2315–20.
12. Winum JY, Dogne JM, Casini A, et al. Carbonic anhydrase inhibitors: synthesis and inhibition of cytosolic/tumor-associated carbonic anhydrase isozymes I, II, IX, and XII with N-hydroxysulfamides – a new zinc-binding function in the design of inhibitors. J Med Chem 2005;48:2121–5.
13. Scozzafava A, Passaponti M, Supuran CT, Gulcin I. Carbonic anhydrase inhibitors: guaiacol and catechol derivatives effectively inhibit certain human carbonic anhydrase isoenzymes (hCA I, II, IX and XII). J Enzyme Inhib Med Chem 2015;30:586–91.
14. Winum JY, Pastorekova S, Jakubickova L, et al. Carbonic anhydrase inhibitors: synthesis and inhibition of cytosolic/tumor-associated carbonic anhydrase isozymes I, II, and IX with bis-sulfamates. Bioorg Med Chem Lett 2005;15:579–84.
15. Cecchi A, Hulikova A, Pastorek J, et al. Carbonic anhydrase inhibitors. Design of fluorescent sulfonamides as probes of tumor-associated carbonic anhydrase IX that inhibit isozyme IX-mediated acidification of hypoxic tumors. J Med Chem 2005; 48:4834–41.
16. De Simone G, Alterio V, Supuran CT. Exploiting the hydrophobic and hydrophilic binding sites for designing carbonic anhydrase inhibitors. Expert Opin Drug Discov 2013;8:793–810.
17. Brown GD, Denning DW, Gow NA, et al. Hidden killers: human fungal infections. Sci Transl Med 2012;4:165rv113
18. Fera MT, La Camera E, De Sarro A. New triazoles and echinocandins: mode of action, in vitro activity and mechanisms of resistance. Expert Rev anti Infect Ther 2009;7:981–98.
19. Wilke M. Treatment and prophylaxis of invasive candidiasis with anidulafungin, caspofungin and micafungin and its impact on use and costs: review of the literature. Eur J Med Res 2011;16:180–6.
20. Ramos PD, Moromi NH, Martínez E, Cadillo E. *Porphyromonas gingivalis*: predominant pathogen in chronic periodontitis. Odontol. Sanmarquina 2011;14:34–8.
21. Vullo D, Del Prete S, Osman SM, et al. Sulfonamide inhibition studies of the γ-carbonic anhydrase from the oral pathogen *Porphyromonas gingivalis*. Bioorg Med Chem Lett 2014;24:240–4.
22. Camí GE, Ramírez de Arellano MC, Fustero S, Pedregosa JC. Synthesis, growth and characterization of new 1,3,4-thiadiazole-5-(*N*-substituted)-sulfonamides crystals. J Arg Chem Soc 2006;94: 5–17.
23. CrysAlisPro, Oxford Diffraction Ltd., Version 1.171.36.20 (release 27-06-2012 CrysAlis171.NET)
24. Sheldrick GM. A short history of *SHELX*. Acta Crystallogr 2008; A64:112–22.
25. Farrugia LJ. *WinGX* suite for small-molecule single-crystal crystallography. J Appl Crystallogr 1999;32:837–8.
26. Spek AL. Single-crystal structure validation with the program PLATON. J Appl Crystallogr 2003;36:7–13.
27. Macrae CF, Edgington PR, McCabe P, et al. Mercury: visualization and analysis of crystal structures. J Appl Crystallogr 2006;39:453–7.
28. Becke AD. Density-functional exchange-energy approximation with correct asymptotic behavior. Phys Rev a Gen Phys 1988;38: 3098–100.
29. Lee C, Yang W, Parr RG. Development of the Colle-Salvetti correlation-energy formula into a functional of the electron density. Phys Rev B Condens Matter 1988;37:785–9.
30. Vosko SH, Wilk L, Nusair M. Accurate spin-dependent electron liquid correlation energies for local spin density calculations: a critical analysis. Can J Phys 1980;58:1200–11.
31. Frisch MJ, Trucks GW, Schlegel HB, et al. Gaussian 09, Revision D.01. Wallingford (CT): Gaussian, Inc.; 2013
32. Bader RFW. Atoms in molecules: a quantum theory. Oxford: Clarendon Press; 1990
33. Bader RFW. A quantum theory of molecular structure and its applications. Chem Rev 1991;91:893–928.
34. Bianchi R, Gervasio G, Marabello D. Experimental electron density analysis of $Mn_2(CO)_{10}$: metal-metal and metal-ligand bond characterization. Inorg Chem 2000;39:2360–6.
35. Bader RFW. 1995. Available from: http://www.chemistry.mcmaster.ca/aimpac/imagemap/imagemap.htm.
36. Biegler-Konig FW, Nguyen-Dang TT, Tal Y, et al. Calculation of the average properties of atoms in molecules. J Phys B 1981;14: 2739–51.
37. Biegler-Konig FW, Bader RFW, Tang T-H. Calculation of the average properties of atoms in molecules. II. J Comput Chem 1982; 13:317–28.
38. Khalifah RG. The carbon dioxide hydration activity of carbonic anhydrase. I. Stop-flow kinetic studies on the native human isoenzymes B and C. J Biol Chem 1971;246:2561–73.
39. Maresca A, Temperini C, Vu H, et al. Non-zinc mediated inhibition of carbonic anhydrases: coumarins are a new class of suicide inhibitors. J Am Chem Soc 2009;131:3057–62.
40. Supuran CT. Carbonic anhydrase inhibitors. Bioorg Med Chem Lett 2010;20:3467–74.
41. Alafeefy AM, Ceruso M, Al-Jaber NA, et al.. A new class of quinazoline-sulfonamides acting as efficient inhibitors against the α-carbonic anhydrase from *Trypanosoma cruzi*. J Enzyme Inhib Med Chem 2015;30:581–5.
42. Carta F, Di Cesare Mannelli L, Pinard M, et al. A class of sulfonamide carbonic anhydrase inhibitors with neuropathic pain modulating effects. Bioorg Med Chem 2015;23:1828–40.
43. GraphPad Prism, Graphpad Software Inc., Copyright 1994–2000 v 3.02. Available from: http://www.graphpad.com/scientific-software/prism/.
44. Carta F, Aggarwal M, Maresca A, et al. Dithiocarbamates: a new class of carbonic anhydrase inhibitors. Crystallographic and kinetic investigations. Chem Commun 2012;48:1868–70.
45. Innocenti A, Vullo D, Scozzafava A, Supuran CT. Carbonic anhydrase inhibitors: interactions of phenols with the 12 catalytically active mammalian isoforms (CA I-XIV). Bioorg Med Chem Lett 2008;18:1583–7.
46. Innocenti A, Vullo D, Scozzafava A, et al. Carbonic anhydrase inhibitors. Interaction of isozymes I, II, IV, V, and IX with carboxylates. Bioorg Med Chem Lett 2005;15:573–8.
47. Di Fiore A, Monti SM, Hilvo M, et al. Crystal structure of human carbonic anhydrase XIII and its complex with the inhibitor acetazolamide. Proteins 2009;74:164–75.
48. Supuran CT. Carbonic anhydrase inhibition/activation: trip of a scientist around the world in the search of novel chemotypes and drug targets. Curr Pharm Des 2010;16:3233–45.
49. Supuran CT. Inhibition of bacterial carbonic anhydrases and zinc proteases: from orphan targets to innovative new antibiotic drugs. Curr Med Chem 2012;19:831–44.
50. Touisni N, Maresca A, McDonald PC, et al.. Glycosyl coumarin carbonic anhydrase IX and XII inhibitors strongly attenuate the growth of primary breast tumors. J Med Chem 2011;54:8271–7.
51. Scozzafava A, Menabuoni L, Mincione F, et al. Carbonic anhydrase inhibitors. Synthesis of sulfonamides incorporating dtpa tails and of their zinc complexes with powerful topical antiglaucoma properties. Bioorg Med Chem Lett 2001;11:575–82.
52. Johnson CK, ORTEP-II. A Fortran thermal-ellipsoid plot program. Report ORNL-5318. Oak Ridge, TN: Oak Ridge National Laboratory; 1976
53. Lin C-C, Hsieh T-H, Liao P-Y, et al. Practical synthesis of *N*-substituted cyanamides via tiemann rearrangement of amidoximes. Org Lett 2014;16:892–5.
54. Prestch E, Clerc T, Seibl J, Simon W. Tablas para la dilucidación estructural de compuestos orgánicos por métodos espectroscópicos: ^{13}CNMR, ^{1}H-NMR, IR, EM, UV-Vis. Barcelona: Singer Verlag-Ibérica; 1998.

55. Koch U, Popelier PLA. Characterization of C-H-O hydrogen bonds on the basis of the charge density. J Phys Chem 1995;99: 9747–54.
56. Supuran CT, Casini A, Mastrolorenzo A, Scozzafava A. COX-2 selective inhibitors, carbonic anhydrase inhibition and anticancer properties of sulfonamides belonging to this class of pharmacological agents. Mini Rev Med Chem 2004;4:625–32.
57. De Simone G, Di Fiore A, Supuran CT. Are carbonic anhydrase inhibitors suitable for obtaining antiobesity drugs? Curr Pharm Des 2008;14:655–60.
58. Supuran CT. How many carbonic anhydrase inhibition mechanisms exist? J Enzyme Inhib Med Chem 2016;31:345–60.
59. Capasso C, Supuran CT. An overview of the alpha-, beta- and gamma-carbonic anhydrases from bacteria: can bacterial carbonic anhydrases shed new light on evolution of bacteria? J Enzyme Inhib Med Chem 2015;30:325–32.
60. Del Prete S, Vullo D, Fisher GM, et al.. Discovery of a new family of carbonic anhydrases in the malaria pathogen *Plasmodium falciparum* - the η-carbonic anhydrases. Bioorg Med Chem Lett 2014; 24:4389–96.

Supplementary material available online